Journal of Biophotonics

JOURNAL OF BIOPHOTONICS

RESEARCH ARTICLE

Zerumbone Induces Apoptosis in Non-Small-Cell Lung Cancer via Biomolecular Alterations: A Microscopic and Spectroscopic Study

Çağla Zübeyde Köprü[1] | Burcu Baba[2] | Dilek Yonar[3]

[1]Faculty of Medicine, Department of Histology and Embryology, Yuksek Ihtisas University, Ankara, Türkiye | [2]Faculty of Medicine, Department of Medical Biochemistry, Yuksek Ihtisas University, Ankara, Türkiye | [3]Faculty of Medicine, Department of Biophysics, Yuksek Ihtisas University, Ankara, Türkiye

Correspondence: Dilek Yonar (dilekyonar@yiu.edu.tr; dilekyonar81@gmail.com)

Received: 14 November 2024 | **Revised:** 16 December 2024 | **Accepted:** 7 January 2025

Funding: This work was supported by the Scientific Research Projects Fund of Yuksek Ihtisas University (project number 2021/01.005).

Keywords: apoptosis | IR spectroscopy | lipid peroxidation | non-small cell lung cancer | zerumbone

ABSTRACT

Zerumbone is a sesquiterpene phytochemical with cytotoxic activity against cancer. This study aimed to evaluate the effect of zerumbone on cell viability by WST-1 test, apoptosis by TUNEL, lipid peroxidation markers (malondialdehyde, MDA, and 4-hydroxynonenal, HNE) by using assay kits, and biomolecular changes by ATR-FTIR spectroscopy in A549 cells. After zerumbone (0–100 μM) incubation for 24, 48, and 72 h, the number of TUNEL-positive cells was found to be higher in zerumbone-treated cells than in controls, in consistent with cell morphology results. MDA levels increased significantly, although HNE levels increased non-significantly in zerumbone-treated cells. Spectral analyses revealed that the zerumbone-treated groups had higher levels of total saturated and unsaturated lipids as well as comparatively shorter-chain lipids. On the contrary, reduced RNA/DNA ratio, total nucleic acid, and protein content were found in zerumbone-treated groups. Consequently, zerumbone-induced apoptosis was accompanied by increased aldehyde products during lipid peroxidation as well as biomolecular alterations.

1 | Introduction

Lung cancer ranks first in cancer-related deaths (18.4% of total cancer deaths) in the world and its effective treatment options remain still poor [1]. Non-small cell lung cancer (NSCLC), the most common type of lung cancer, has limited treatment options such as surgery and chemotherapy [2]. Chemotherapeutics used today are insufficient to destroy the tumor or prevent its recurrence and cause many side effects [2]. Patients with advanced NSCLC respond to cisplatin, the first generation of platinum-based drugs. However, the development of drug resistance significantly restricts the efficacy of cisplatin. One of the main causes of cisplatin resistance in NSCLC has been found to be defects in apoptotic signal transduction [3]. Natural compounds that do not cause toxicity in normal cells, can inhibit the growth of cancer cells and have an apoptotic effect on these cells. Therefore, they can be used as new anti-carcinogenic agents [3–5]. In recent studies, the use of natural compounds such as zerumbone attracts attention [3, 5–7].

Zerumbone is an organic compound extracted from *Zingiber zerumbet (L.) Smith* rhizomes [8]. It has been used in the treatment of many diseases (stomachache, toothache, fever and indigestion) worldwide [5, 9, 10]. Zerumbone exhibits antiproliferative, anti-metastatic and pro-apoptotic properties against some types of cancer [11, 12]. Since studies to date have revealed the anticarcinogenic effects of zerumbone in many

Abbreviations: ATR-FTIR, attenuated total reflectance-Fourier transform infrared; HNE, 4-hydroxynonenal; MDA, Malondialdehyde; NSCLC, non-small cell lung cancer; TUNEL, terminal deoxynucleotidyl transferase-mediated dUTP nick end labeling; ZER, Zerumbone.

types of cancer (liver, breast, leukemia, cervix, ovary, pancreas, prostate, and lung cancer), it was found to have better cytotoxic effects and cancer cell selectivity than cisplatin and is considered as a promising agent [3, 9, 11, 13–19].

Triggering apoptosis is an important mechanism of action in the use of anticancer agents. It is known that zerumbone induces apoptosis through events such as loss of mitochondrial membrane potential, release of cytochrome c, activation of caspase-3 and caspase-9, increased expression of p53 and Bax, and increased reactive oxygen species (ROS) production [6, 20]. ROS that initiate lipid peroxidation plays a role in the formation of cancer cells. The products formed as a result of peroxidation are involved in signaling pathways, proliferation, differentiation and apoptosis in the cell [21]. Malondialdehyde (MDA) and 4-hydroxynonenal (HNE) resulting from the peroxidation of polyunsaturated fatty acids have attracted more attention [22]. MDA is regarded as the most mutagenic byproduct of lipid peroxidation, while 4-HNE appears to be the most toxic one [23, 24]. Both MDA and HNE have been implicated in pathological conditions such as cancer [22]. Therefore, it is important to evaluate the levels of lipid peroxidation products, MDA and HNE, and also the effects of zerumbone on these markers in lung cancer cells.

Determining the possible structural and relative changes in biomolecules is important to elucidate the action mechanism of compounds that can be used in cancer treatment. Infrared (IR) spectroscopy has been widely used to detect and differentiate different types of cancer cells based on spectral differences, as it elucidates the biochemical composition of cells [25–28]. It detects not only the chemical nature of biomolecules, but also their conformations. It has the potential to provide fast, sensitive and simultaneous monitoring of biological specimens without destroying the sample. In addition, this technique is also used to discriminate drug-resistant and drug-sensitive cancer cells and to determine apoptosis in cancer cells [29].

Studies investigating the effects of zerumbone on lung cancer are limited [3, 5, 10, 30]. Its exact mechanism has not been fully clarified. In the present study, we investigated the cell viability and apoptotic activity of zerumbone on human NSCLC. In addition, we determined the levels of MDA and HNE as lipid peroxidation markers, and also the alterations in the biomolecules of NSCLC cells using Fourier transform infrared (FTIR) spectroscopy after zerumbone treatment. The effects of zerumbone on cancer cells using FTIR spectroscopy were explored for the first time, which could provide new insights into cancer treatment. The results obtained will contribute to molecular studies that can be performed with zerumbone in the future.

2 | Experimental Section

2.1 | Cell Culture

Human lung cancer A549 (ATCC CCL-185) cell line was cultured in Dulbecco's modified Eagle's medium (DMEM-HG) supplemented with 10% fetal bovine serum (FBS), 1% antibiotic (penicillin–streptomycin) and incubated at 37°C in a humidified incubator with 5% CO_2. The medium of the cells was replaced with fresh medium every 3–4 days.

2.2 | Zerumbone Treatment

Zerumbone was prepared in basal medium containing 0.01% dimethyl sulphoxide (DMSO). After cells reached 70% confluency, cells were treated with different concentrations of zerumbone (0–100 μM). Cell viability was determined by WST-1 Assay (cat. no: 5015944001, Roche, Switzerland). Culture medium containing 0.01% DMSO was used as the negative control.

2.3 | Cell Viability Assay

Cells were cultured at a density of 5×10^3 cells/well in 96 well plates with different concentrations of zerumbone and incubated for 24, 48, and 72 h. After incubation, 10 μL of WST-1 reagent was added to wells and the absorbance was measured at 450 with 620 nm reference wavelength using the ELISA reader (Biotek Epoch 2, Agilent, USA).

$$\text{Percentage of cell viability (\%)} = (\text{Optical density (OD) of treated cells}/\text{OD of untreated cells})\times 100$$

2.4 | AO/PI Staining

To determine the apoptotic properties of zerumbone-treated A549 cells, acridine orange (AO) (cat. no: 212536, BD, USA) and propidium iodide (PI) (cat. no: 81845, Sigma–Aldrich, USA) were used to stain the cells. Briefly, cells were cultured in 6-well plates and treated with different zerumbone concentrations (80, 60, and 50 μM) for 24, 48, and 72 h. After trypsinization, the cells (2×10^6 cells/mL) were centrifuged at 1200 rpm for 5 min and the supernatant was discarded. The tubes were kept on ice until the staining process. 10 μL PI (1 mg/mL) and 1 μL AO (10 mg/mL) dyes were added to the cell pellet and incubated at room temperature for 15 min. After incubation in the dark, a drop was taken from the suspension and placed on a glass slide and examined with a fluorescent microscope (Olympus IX35, Japan). The same procedure was applied to the cells that were not treated with zerumbone used as a control.

2.5 | TUNEL Assay

To evaluate cell death by apoptosis, In Situ Cell Detection Kit (cat. no: 11684817910, Roche, Switzerland) was used according to the manufacturer's protocol. In brief, cells were cultured with zerumbone for 48 h. Then fixation (with paraformaldehyde of 4%), blocking (with H_2O_2 of 0.3%) and permeabilization (with triton X-100 of 0.1% containing sodium citrate of 0.1%) were done. After addition of label and enzyme solutions, the samples were incubated at 37°C for 60 min. Nucleus staining was performed with DAB Substrate Kit (cat. no: ab64238, Abcam, UK) and counterstaining was performed with hematoxylin. The samples were mounted and examined under a light microscope (Olympus CKX53, Japan). The apoptotic index was calculated by counting a minimum of 100 cells for each sample.

$$\text{Apoptotic index} = (\text{Number of dead cells} / \text{Total number of cells})\times 100$$

2.6 | Measurement of Lipid Peroxidation

The levels of MDA as an indicator of lipid peroxidation were measured using an assay kit (cat. no: ab118970, Abcam, UK) according to the manufacturer's protocols. After treatment, A549 cells were washed with cold phosphate buffer saline (PBS) and then, homogenized with MDA lysis buffer containing butylated hydroxytoluene. The samples were centrifuged at 13 000 *g* at 4°C for 10 min and the supernatant was taken. MDA concentrations were measured by a method based on the reaction of MDA with TBA (2-thiobarbituric acid). MDA levels were expressed as nmol/mg protein. The protein concentrations were determined by the Bradford method [31]. The 4-HNE ELISA Kit (cat. no: E-EL-0128, Elabscience, USA) was used to determine the levels of HNE, which is a marker of lipid peroxidation. Briefly, 4-HNE in the samples were probed with biotinylated detection antibody specific to 4-HNE, followed by incubation with avidin conjugated to horseradish peroxidase. The levels of 4-HNE were determined by comparing the OD of the samples to the standard curve. HNE levels were expressed as pmol/mg protein.

2.7 | ATR-FTIR Spectroscopy

A549 cells (2×10^6 cells/mL) were re-suspended in 10 μL PBS for ATR-FTIR analysis. The IR spectra of A549 cells treated with zerumbone and control (untreated cells) were collected with the one-bounce attenuated total reflectance mode of a Perkin Elmer Frontier model FTIR spectrometer (Perkin Elmer Inc., USA) equipped with a Quest single reflection ATR accessory (Specac Ltd., UK). The cells were directly placed onto the ATR crystal. Drying with a mild flow of N_2 gas was applied to remove water in PBS for 10 min. The cell films were obtained from five independent experiments for each group. ATR-FTIR spectra were collected in the 4000–450 cm^{-1} region with 64 scans and 4 cm^{-1} resolution at room temperature and used for spectral analysis. The average spectra obtained for each group were baseline corrected and normalized to the amide A band for visual representation. The qualitative and quantitative differences in the molecular composition of cells can be obtained by the position and the area of the characteristic bands by IR spectroscopy. The area of the characteristic bands is directly proportional to the concentration of the relevant molecule according to the Beer–Lambert law. The integrated area ratios of some specific bands were evaluated to eliminate the artifacts caused by experimental conditions and to show relative quantitative analysis.

2.8 | Statistical Analysis

Statistical analyses were performed with GraphPad Prism (GraphPad Software Inc., USA). The normality of the data was analyzed by the Kolmogorov–Smirnov test. One-way ANOVA with Tukey's post hoc test was used for comparison of multiple groups. The results were presented as mean ± SEM. Significance was considered as $^*p<0.05$, $^{**}p<0.01$, and $^{***}p<0.001$.

3 | Results and Discussion

3.1 | Effect of Zerumbone on Cell Viability

The effect of zerumbone on cell viability was examined in A549 cells. The WST-1 assay revealed that zerumbone treatment for 24, 48, and 72 h causes a significant decrease in cell viability in a dose-dependent manner. The half maximal inhibitory concentration (IC_{50}) values for 24, 48, and 72 h were found 80, 60, and 50 μM, respectively (Figure 1). Our findings demonstrated that IC_{50} values were changing according to incubation times in a dose-dependent manner. It was concluded that the exposure to zerumbone for a longer incubation time leads to inhibition of cell growth and viability at a lower dose, which is consistent with previous studies [5, 32].

3.2 | Zerumbone Affects Morphology of A549 Cells

Morphological changes of A549 cells after zerumbone treatment were examined by AO/PI staining method. It was observed that the density of live cells was higher with AO staining (green color) and showed normal morphology (Figure 2A). After treatment with zerumbone, it was observed that early properties such as chromatin condensation and membrane blebbing were increased. Changes in these properties from the 24th hour to the 72nd hour increase the probability of necrosis in cells with long-term exposure to zerumbone. At the end of the 72nd hour, the late apoptotic stage appears in a red-orange color due to the binding of PI to denatured DNA (Figure 2B–D).

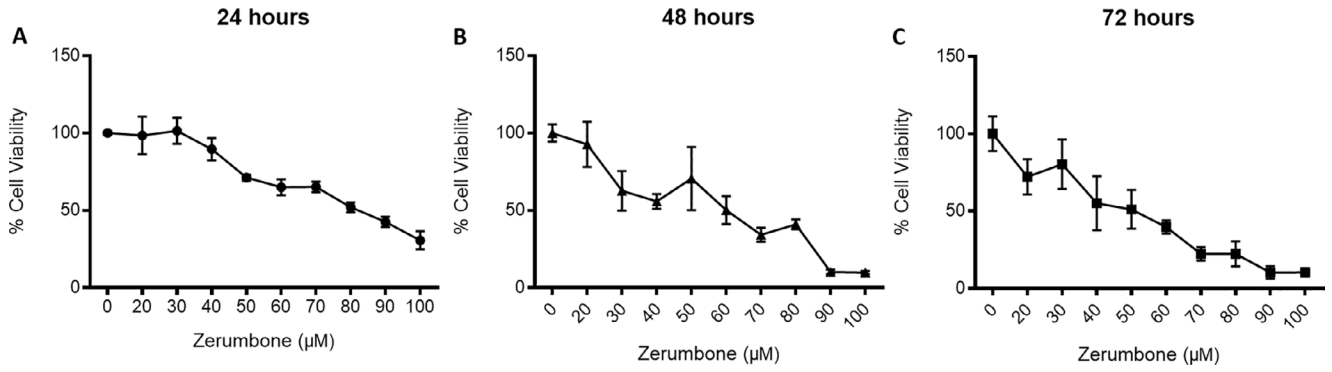

FIGURE 1 | Effect of zerumbone at different concentrations (0–100 μM) on the cell viability of A549 cells after (A) 24 h, (B) 48 h, and (C) 72 h incubation periods (the results are expressed as the mean ± SEM of three independent experiments).

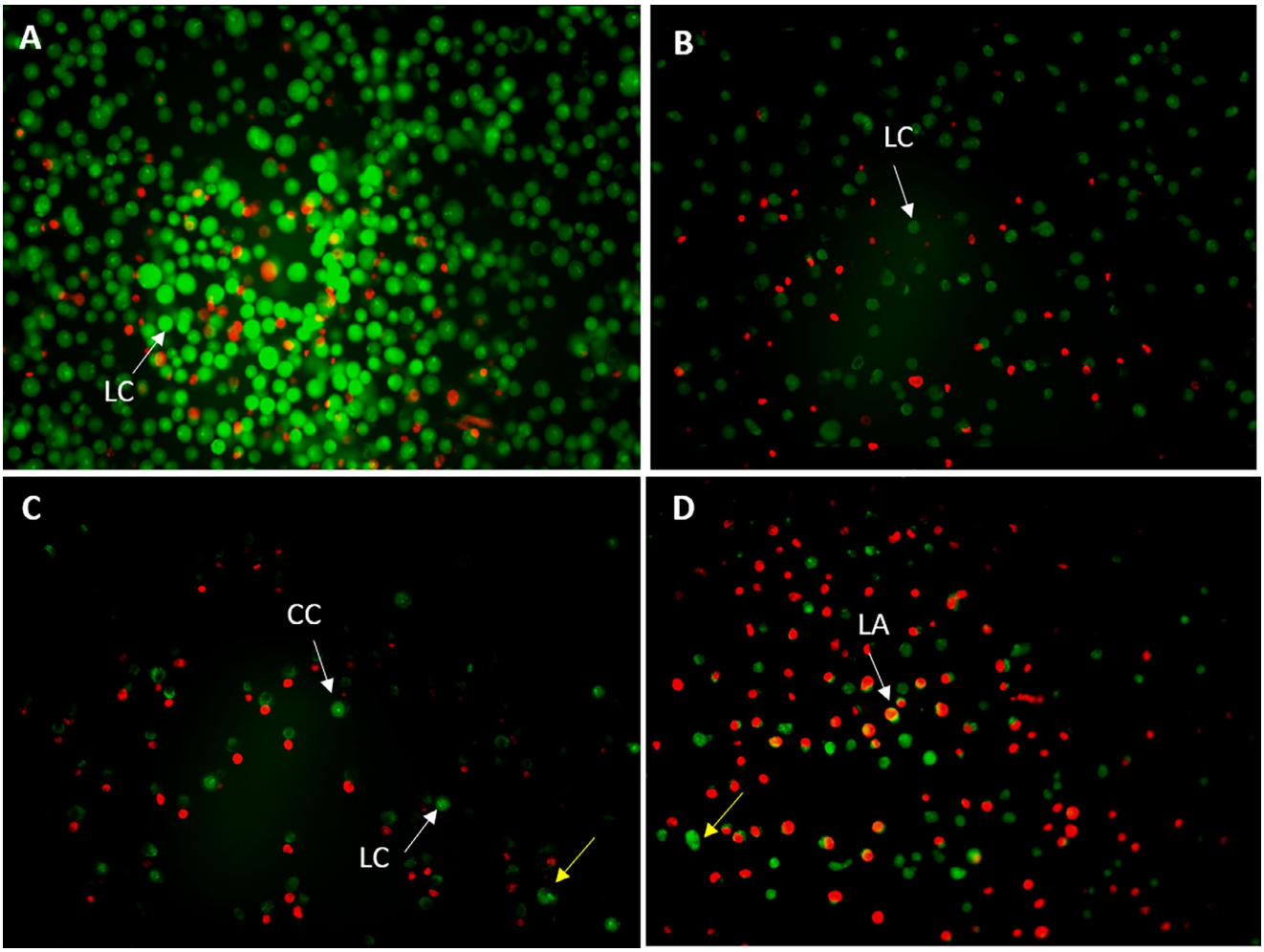

FIGURE 2 | Fluorescence microscope images of A549 cells stained with AO and PI. (A) A549 cells not treated with ZER were healthy (magnification: 200×). After (B) 24 h and (C) 48 h post-treatment with ZER, early apoptotic features, including cell membrane blebbing (yellow arrow) and chromatin condensation, were observed (magnification: 100×). (D) Signs of late apoptosis were observed after 72 h ZER treatment (magnification: 200×). CC: chromatin condensation; LA: late apoptosis; LC: living cells.

According to our results, zerumbone lead to morphological changes associated with apoptosis in A549 cells depending on time, as expected. Similar to our study, Nathaniel et al. reported that there were apoptotic figures in the cells treated with zerumbone for 72 h in colorectal cancer with AO/PI staining [33]. In another study conducted with breast cancer cells, AO/PI staining showed that zerumbone caused early and late apoptotic features after 72 h [34].

3.3 | Zerumbone Treatment Induces Apoptosis

TUNEL assay was performed to investigate whether zerumbone treated A549 cells go through apoptosis. TUNEL method allows us to examine the early stages of apoptosis [35]. In this method, DNA breaks in the apoptotic cell nucleus react with DAB and appear brown, while non-apoptotic cells appear purple as a result of counterstaining with hematoxylin. The number of TUNEL positive cells was found to be higher in A549 cells (46.3%) treated with zerumbone for 48 h than the control cells (3.7%) ($p < 0.0001$). According to TUNEL results, apoptotic cells increased in zerumbone-treated cells compared to control (Figure 3).

Our data indicates that apoptotic cell death increases due to zerumbone treatment, consistent with previous studies on colorectal [33], breast [16, 36], prostate [32], and lung cancer cells [3, 5]. Previous studies on breast and colorectal cancers have shown the anticancer effects of zerumbone and zerumbone-loaded nanostructured lipid carriers [16, 33]. Zerumbone induced apoptosis via caspase-dependent pathway in prostate cancer [32]. Several studies also reported that zerumbone induces apoptosis in NSCLC [3, 5]. It was demonstrated that zerumbone and cisplatin inhibited the growth of NSCLC cells. Even, zerumbone (20.9%) induced apoptosis more than cisplatin (7.8%), leading to an almost 3-fold increase in apoptosis [3]. The studies conducted emphasize the cytotoxic effect of zerumbone in cancer cells, consistent with our findings.

3.4 | Lipid Peroxidation Increases After Zerumbone Treatment in A549 Cells

Lipid peroxidation reactions are induced as a result of excess ROS formation, resulting in high generation of reactive aldehydes and their derivatives including MDA and 4-HNE [24]. The main lipid peroxidation product, MDA can promote

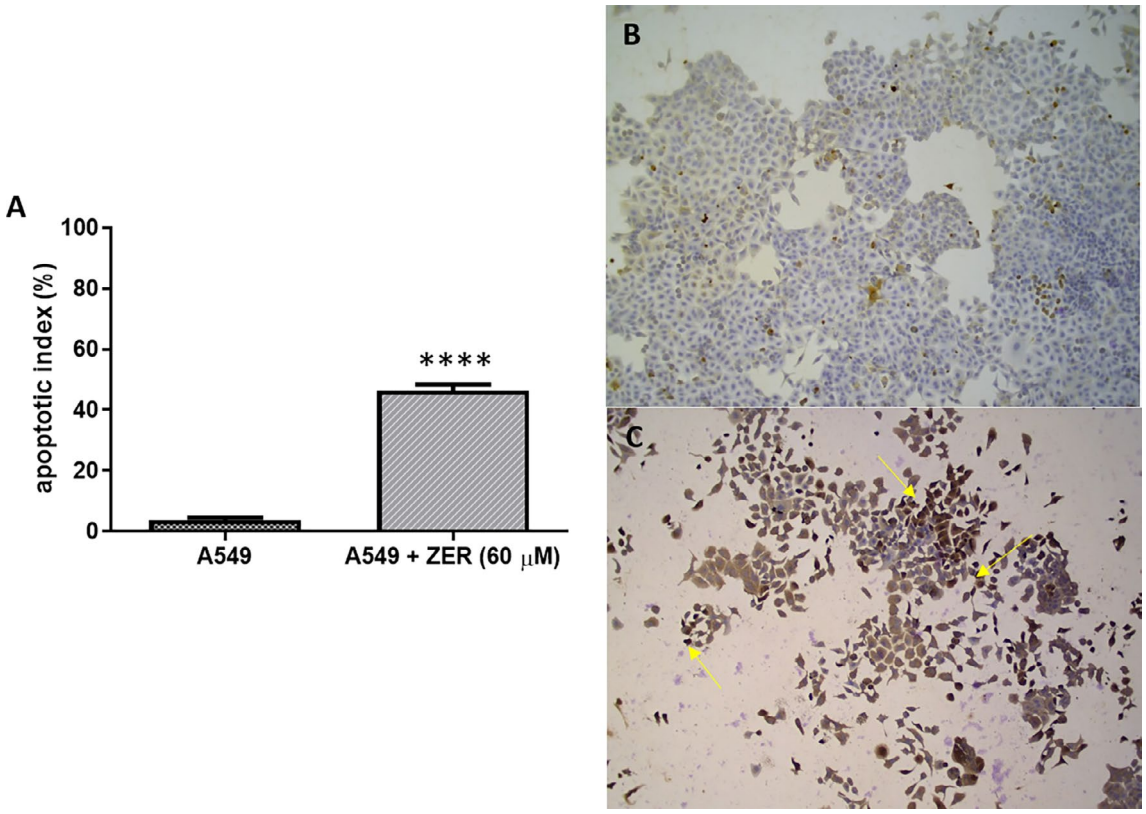

FIGURE 3 | Apoptotic index graphs and micrographs after ZER treatment of A549 cells by the TUNEL method. (A) Apoptotic index graph of ZER-treated cells compared to untreated cells (****$p < 0.0001$). (B) Light microscope images of control cells as a result of TUNEL staining (×10). (C) Light microscope images of ZER-treated cells resulting from TUNEL staining (×10). Yellow arrows indicate TUNEL positive cells with brown nuclei. Counterstaining was done with hematoxylin. TUNEL: terminal deoxynucleotidyl transferase-mediated dUTP nick end labeling.

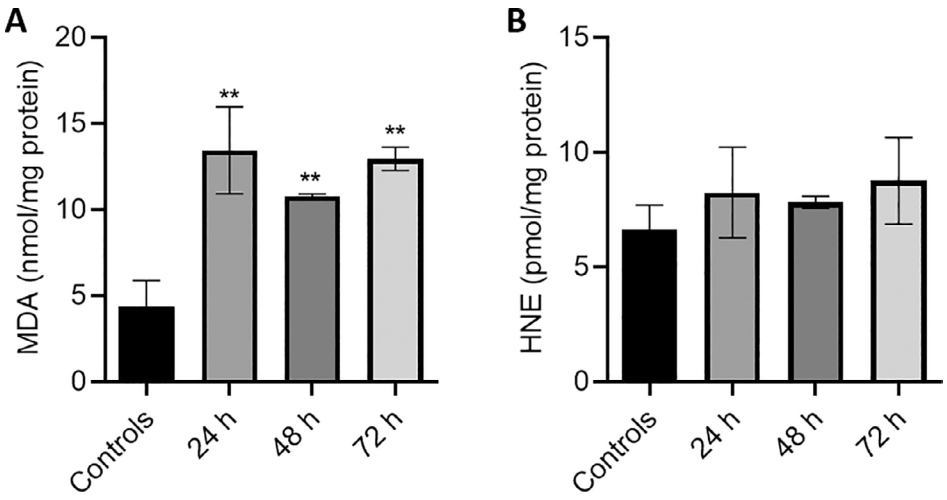

FIGURE 4 | Effects of zerumbone on MDA and HNE levels. (A) The effect of zerumbone treatment on MDA levels in A549 cells at the 24, 48, and 72 h (80, 60, and 50 μM, respectively, $p < 0.01$). (B) The effect of zerumbone treatment on HNE levels in A549 cells at 24, 48, and 72 h (80, 60, and 50 μM, respectively, $p > 0.05$) (Graphs represent the results of three independent experiments with mean ± SEM).

protein/DNA crosslinking that may stimulate alteration in the biomolecules and also accumulate during aging and in chronic diseases. In addition, it can modify significant proteins and could contribute to reduction of protein synthesis [23, 37]. The aldehyde compound 4-HNE is also highly reactive and generates adducts with cellular proteins and DNA [24]. Elevated 4-HNE levels can react with proteins and/or DNA to generate adducts that lead to various cytotoxic and genotoxic outcomes [23].

In our study, MDA and HNE concentrations in A549 cells were evaluated at IC_{50} values of different incubation times. MDA levels were higher in the groups treated with zerumbone when compared to controls ($p < 0.01$). The levels of HNE tended to increase

in the zerumbone-treated groups compared to controls. However, no statistically significant difference was detected ($p > 0.05$) (Figure 4). Consistent with our findings, Bianchi et al. showed that curcumin, another natural compound from ginger family, induces apoptosis in cancer cells by promoting the formation of MDA [38]. Additionally, similar to our results, it was reported that the MDA levels increased in the lung tumor model after zerumbone treatment compared to control [39]. Contrary to these studies and our results, Yao et al. found that curcumin treatment caused a decrease in MDA and HNE levels in A549 cells [40].

Our results demonstrated that zerumbone administration may increase lipid peroxidation, leading to irreversible damage that induces the apoptotic pathway in A549 cells. Zerumbone treatment caused an increase in lipid peroxidation products, suggesting that zerumbone may overcome antioxidant defenses and drive cancer cells to apoptosis.

3.5 | Zerumbone Changes Cellular Biomolecular Content

In this study, ATR-FTIR spectroscopy was used to follow structural and compositional alterations in biomolecules of all groups at different incubation times. The averages of the baseline corrected normalized IR spectra of all groups and

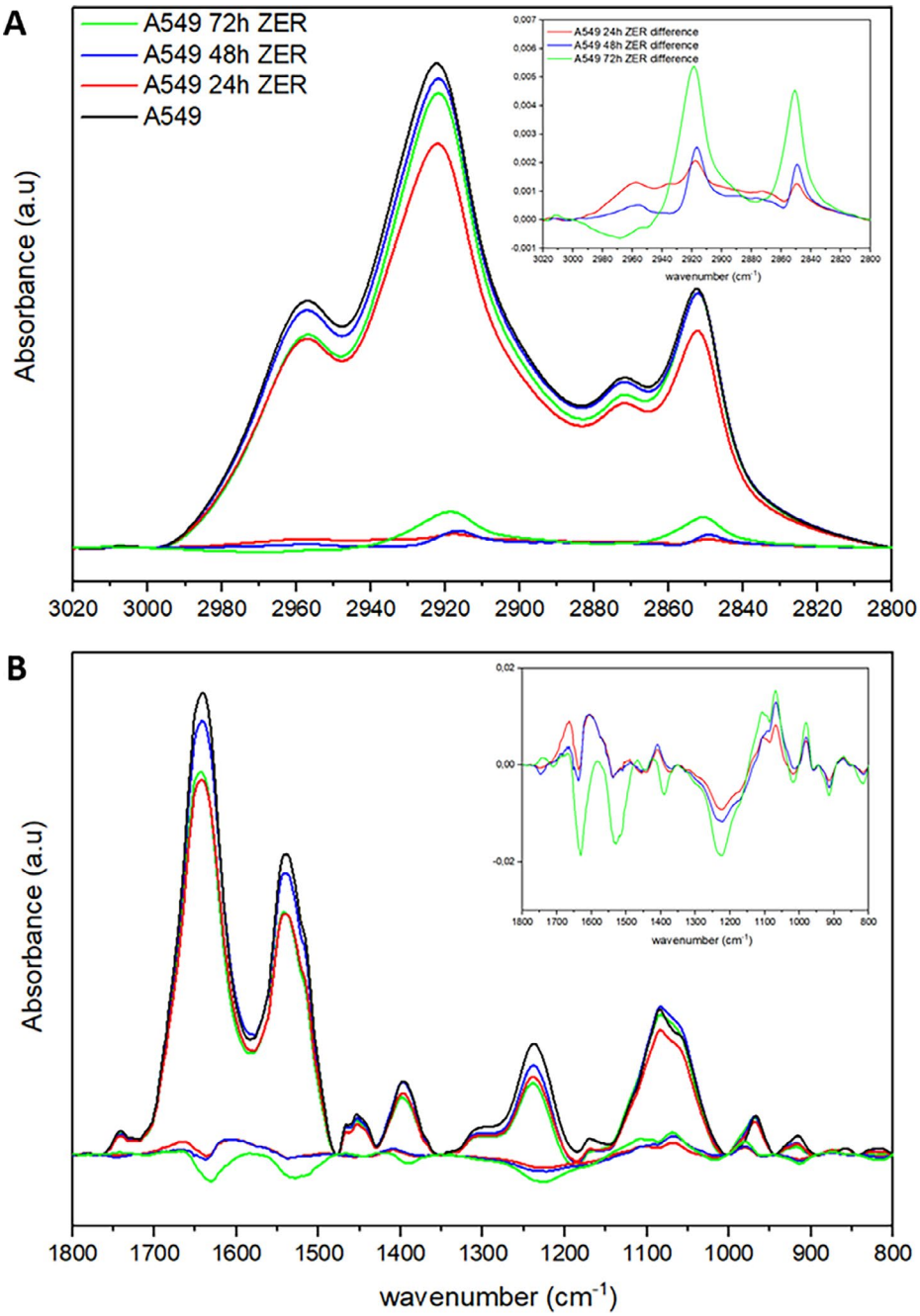

FIGURE 5 | Average FTIR spectra of control (untreated A549 cells) and ZER-treated A549 cells for 24, 48, and 72 h (A) 3020–2800 cm^{-1} region, (B) 1800–800 cm^{-1} region (baseline corrected, normalized with respect to Amide A). Difference IR spectra were obtained by the subtraction of the control spectrum from the treated cells' spectra in the subpanels for both regions.

TABLE 1 | Band assignments of major absorptions in IR spectrum of A549 cells [42–44].

Wavenumber (cm^{-1})	Band assignments
3008	Olefinic =CH stretching: unsaturated lipids
2957	CH_3 antisymmetric stretching: protein, lipid
2922	CH_2 antisymmetric stretching: mainly lipid
2872	CH_3 symmetric stretching: mainly protein
2853	CH_2 symmetric stretching: mainly lipid
1740	Ester C—O stretching: triglyceride, cholesterol ester
1640	Amide I: protein (mostly due to C=O stretching vibration of amide groups)
1540	Amide II: protein (60% N—H bending, 40% C—N stretching)
1469	CH_2 bending: lipid
1453	CH_3 antisymmetric bending: mainly lipids and little contribution from proteins
1398	COO^- symmetric stretching: fatty acids and amino acids
1307	Amide III: C—N stretching and N—H bending
1238	PO_2^- antisymmetric stretching: mainly nucleic acids with minor contribution of phospholipids
1170	CO—O—C antisymmetric stretching: ester bonds in cholesteryl esters
1118	C—O stretching: ribose ring vibrations (RNA)
1084	PO_2^- symmetric stretching: nucleic acids and phospholipids; C—O stretching: polysaccharide and glycolipid
1055	C—O stretching: polysaccharide (glycogen)
968	C—C/C—O stretching: DNA (deoxyribose and phosphate moieties of DNA backbone)
915	Bending vibrations of carboxylic acid groups/ribose ring vibrations (RNA)

the difference spectra, in which the average spectrum of each zerumbone-treated A549 cells was subtracted from the average spectrum of the untreated A549 cells (control) in the 3020–2800 cm^{-1} (C—H region) and 1800–800 cm^{-1} (fingerprint region) wavenumber range are shown in Figure 5. Different functional groups in the biomolecules such as lipid, protein, nucleic acid, and carbohydrate create characteristic absorption bands in the IR spectrum of biological specimens [41]. The assignments of the spectral bands related to the functional groups of biomolecules according to the related literature [42–44] are given in Table 1. The area ratios of some specific spectral bands were calculated to analyze zerumbone-induced changes in A549 cells (Table 2).

Infrared spectra have been used for the observation of various lipids, structural details of biomembranes [42, 45] and lipid self-assemblies [46, 47]. Absorptions in the 3020–2800 cm^{-1} region arising from the olefinic =CH stretching, the antisymmetric and symmetric stretching of methylene ($—CH_2$) and methyl ($—CH_3$) groups were monitored to evaluate the changes in lipid content of the cells such as saturated and unsaturated lipid content, chain length, order and dynamics. The antisymmetric and symmetric stretching of methylene groups (around 2922 and 2852 cm^{-1}, respectively) originate from the long hydrocarbon chains in lipids and their total area corresponds to the saturated lipid content. The saturated lipid content increased in zerumbone-treated groups. The unsaturated/saturated lipid ratio provides an unsaturation index indicating the double bond content in the lipid structure. This ratio tended to increase in the 24 and 48 h zerumbone-treated groups compared to controls, suggesting the increased lipid peroxidation in ZER-treated groups. However, a slightly similar value was found with control group in this ratio for the 72 h zerumbone-treated groups (Figure 6A). The methyl/methylene area ratio represents the changes in the acyl chain length. A higher value of this ratio indicates the presence of relatively shorter chains and/or more branched lipids, resulting in lipid peroxidation. Figure 6B shows the increased methyl/methylene area ratio in the 24 and 48 h zerumbone-treated groups, but no significant changes were observed in this ratio. However, this ratio was also found slightly similar to control group for the 72 h zerumbone-treated groups. The prolonged exposure of cells to zerumbone suggests that they can deal with lipid peroxidation. The carbonyl (C=O)/lipid and ester CO—O—C/lipid ratios yield the triglyceride and cholesterol ester content. Significant reductions in these ratios were found for zerumbone-treated groups in comparison with control (Figure 6C,D). Total lipids demonstrated a significant increase in zerumbone-treated groups, which may be used as a defense mechanism to counteract oxidative damage. Moreover, we observed a higher unsaturation index by zerumbone treatment. It was supported by our lipid peroxidation results (Figure 4). Zerumbone may increase lipid peroxidation and cause oxidative damage by changing lipid content in cancer cells.

The order/disorder state of lipids (lipid acyl chain flexibility) can be decided by the shifts in the frequencies of the antisymmetric and symmetric CH_2 stretching vibrations [48]. The peak positions of these bands significantly shifted to lower wavenumber values in zerumbone-treated groups (Table 3), which indicates increased number of *trans* conformers of lipids. Thus, zerumbone caused elevated lipid order and reduced acyl chain flexibility. The changes in the lipid order may alter cell shape, hence changing the thickness of the cell membrane. The alterations in lipid order can modify crucial cellular activities such as signaling pathways and transport of molecules [42].

Changes in protein amount are calculated by the total areas of amide I (1640 cm^{-1}) and amide II (1538 cm^{-1}) bands. There was a slight decrease in total protein content of zerumbone-treated

TABLE 2 | The IR band area ratios of some functional groups and their indications.

Area ratio	Biomolecular origin	Indication
A_{2957}/A_{2922}	$\upsilon_{as}(CH_3)/\upsilon_{as}(CH_2)$	Aliphatic chain length
$A_{3008}/A_{2922+2853}$	$\upsilon(=CH)/\upsilon_{as}(CH_2)+\upsilon_{s}(CH_2)$	Unsaturation index
$A_{1740}/A_{2922+2853}$	Ester $\upsilon(C=O)/\upsilon_{as}(CH_2)+\upsilon_{s}(CH_2)$	Triglyceride-cholesterol ester amount
$A_{1170}/A_{2922+2853}$	Ester $\upsilon_{as}(CO-O-C)/\upsilon_{as}(CH_2)+\upsilon_{s}(CH_2)$	Cholesteryl ester amount
A_{1640}/A_{1540}	Amide I/amide II	Protein structural and conformational changes
$A_{2922+2853}/A_{1640+1540}$	$\upsilon_{as}(CH_2)+\upsilon_{s}(CH_2)$/amide I + amide II	Lipid/protein content
$A_{1238+1084}/A_{1640+1540}$	$\upsilon_{as}(PO_2^-)+\upsilon_{s}(PO_2^-)$/amide I + amide II	Nucleic acid/protein content
$A_{1055}/A_{1640+1540}$	$\upsilon(C-O)$/amide I + amide II	Glycogen/protein content
A_{1118}/A_{968}	$\upsilon(C-O)/\upsilon(C-C)$ or $\upsilon(C-O)$	RNA/DNA content

Abbreviations: as = antisymmetric; s = symmetric; υ = stretching.

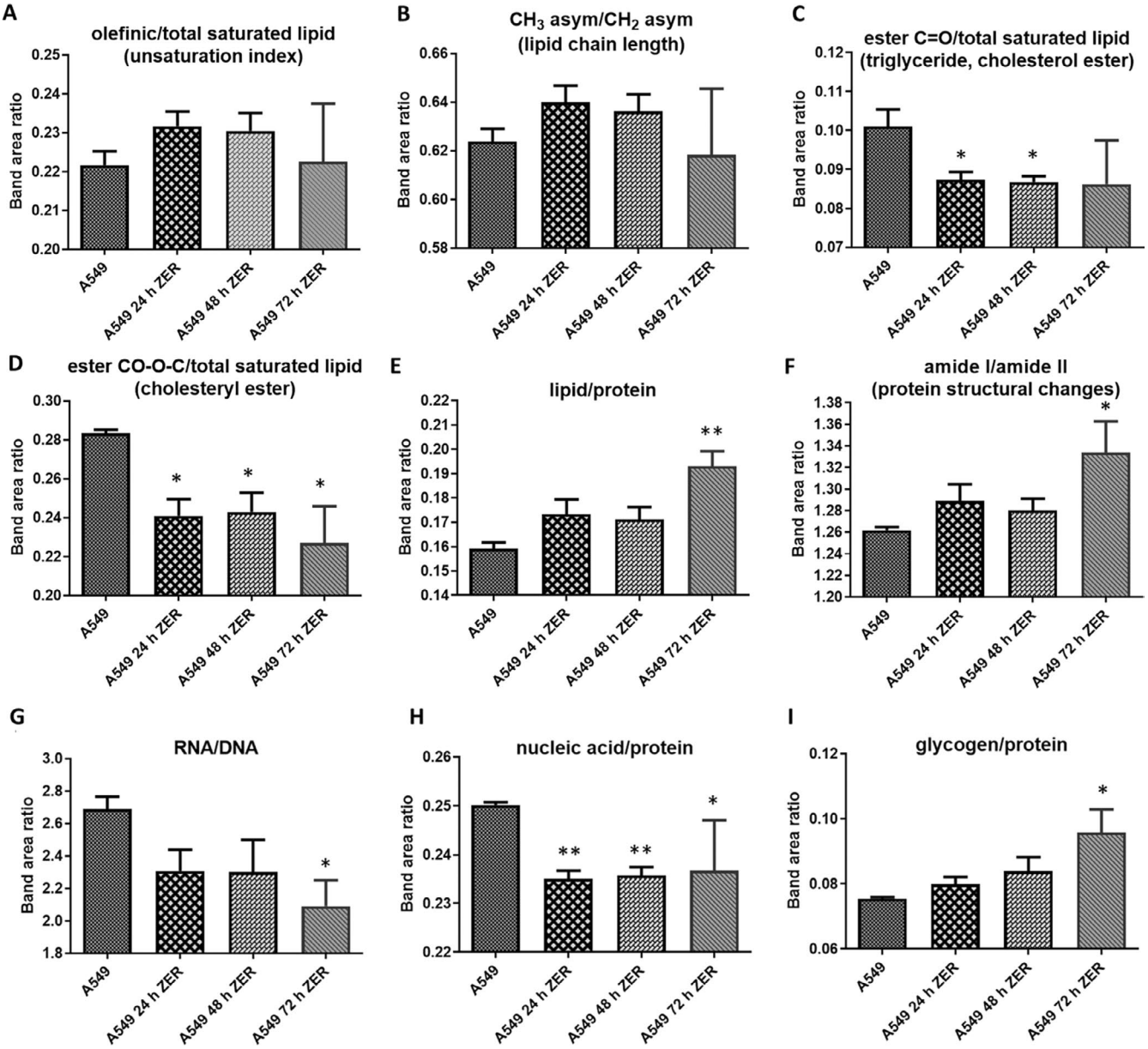

FIGURE 6 | IR band area ratios in control and ZER-treated A549 cells for 24, 48, and 72 h (A) olefinic/saturated lipid, (B) ester C=O/saturated lipid, (C) ester CO—O—C/saturated lipid, (D) CH_3 antisym/CH_2 antisym, (E) lipid/protein, (F) amide I/amide II, (G) RNA/DNA, (H) nucleic acid/protein, (I) glycogen/protein (the significance levels were denoted as $^*p < 0.05$ and $^{**}p < 0.01$).

TABLE 3 | Changes in the wavenumbers of saturated lipid functional groups and protein amide I and amide II bands.

	Wavenumber (cm^{-1})			
	Untreated A549 cells	ZER-treated A549 cells		
Band	**Control**	**24 h**	**48 h**	**72 h**
CH_2 antisymmetric stretching	2922.71 ± 0.09	2922.49 ± 0.02	2922.22 ± 0.07 ***	2922.20 ± 0.11 **
CH_2 symmetric stretching	2852.67 ± 0.03	2852.50 ± 0.02 *	2852.32 ± 0.04 ***	2852.39 ± 0.07 **
Amide I	1639.98 ± 0.18	1641.51 ± 0.88	1640.81 ± 0.43	1642.55 ± 0.64
Amide II	1538.74 ± 0.91	1538.52 ± 0.36	1539.61 ± 1.00	1540.51 ± 1.04

Note: The significance levels were denoted as *$p < 0.05$, **$p < 0.01$, and ***$p < 0.001$.

groups. The lipid/protein ratio in zerumbone-treated cells increased compared to the control group indicating the change in lipid and protein metabolism (Figure 6E). It may be attributed to increased lipids or decreased protein content.

Amide I/amide II area ratio and changes in the frequencies of these amide bands are sensitive to structural and conformational changes of the proteins. A slight increase in the wavenumber of the amide I and II bands in zerumbone-treated cells shows alterations in protein conformation (Table 3). Additionally, the increase in the amide I/amide II area ratio represents the structural variations in proteins during apoptosis (Figure 6F).

Nucleic acids are of vital importance as they undergo changes in diseases such as cancer, where cell division and growth are affected. The DNA replication and transcription processes during carcinogenesis may result in enhanced signals from unwound DNA. Also, increased signals can arise from RNA during transcription and translation in cancer cells compared to normal cells [49]. The vibrations from PO_2^- functional groups at around 1084 and 1238 cm^{-1} originate mainly in the phosphodiester groups of nucleic acids (Figure 5 and Table 1). Integrating the symmetric and antisymmetric vibrations of PO_2^- functional groups corresponds to the nucleic acid content. RNA/DNA ratio is a parameter with diagnostic potential in different types of malignancies in previous studies [48, 50]. High RNA/DNA ratio in controls tended to decrease in zerumbone-treated cells, which may be due to apoptosis induced by zerumbone (Figure 6G). The nucleic acid/protein ratio given in Figure 6H demonstrates a decrease in the amount of nucleic acid in zerumbone-treated cells compared to control. Since there is a slight decrease in the total protein content, it can be concluded that the decrease in the nucleic acid amount is greater than the decrease in the protein amount. Zerumbone may cause a decrease in the amount of nucleic acid by intercalating with the DNA molecule and preventing DNA replication, as reported in the study by Fale et al. with doxorubicin [51]. In a study on HL60 cells conducted by Gasparri and Muzio, it was reported that the nucleic acid/protein ratio was inversely correlated with the apoptotic index [52]. The decrease in the nucleic acid/protein ratio after treatment with zerumbone might be associated with an increased apoptotic index, which is consistent with our TUNEL results (Figure 3). The area ratio A1238/A1084 describes the structural changes of nucleic acids, which decreased in zerumbone-treated cells compared to control (2.912 and 3.436, respectively, $p < 0.05$). Reactive species may attack both the deoxyribose and bases of DNA through oxidative and nitrative modifications, which can alter the structural integrity and biological functions of nucleic acids, potentially leading to cell apoptosis [53].

Protein and nucleic acids are prone to be modified by lipid peroxidation products [23]. The adduction of lipid peroxidation-derived aldehydes to DNA results in the formation of bulky adducts, which contribute to genome instability. These bulky DNA adducts play a crucial role in mutagenesis and carcinogenesis [54]. The mutational spectrum of MDA is associated with DNA interaction leading to the generation of guanosine, adenosine, and cytidine adducts [55]. In addition, HNE binds to proteins and may alter cellular signaling and transcription in a concentration-dependent manner. At high concentrations, HNE make cells more vulnerable to additional mutagenic and carcinogenic exposures by preventing the repair of bulky adducts. Furthermore, elevated HNE levels in cells promote apoptotic signaling [56]. The increment in MDA and HNE levels in our findings suggest that these products may disrupt cellular processes such as protein and DNA synthesis, through covalent modifications of proteins and DNA. Therefore, it may lead to a reduction in protein and nucleic acid content observed in the zerumbone-treated groups.

Glycogen is a crucial energy store in cancer cells and its turnover helps cells for adaptation and survival under adverse oxygen and nutrient circumstances. Glycogen content has been shown to be inversely proportional to the proliferation rate in various cancer cells and tumors [57]. The area ratio demonstrating the glycogen level with respect to the protein amount was lower in A549 cells and increased by zerumbone treatment (Figure 6I). An increase in the glycogen level indicates a decrease in proliferation, as stated by Zois et al. [57].

The results of FTIR spectroscopy showed the changes in the content and structure of biological molecules in A549 cells induced by zerumbone. Furthermore, the molecular changes occurring at different incubation times suggest that long-term exposure to zerumbone (72 h) may have caused cells to become resistant.

4 | Conclusion

Our data suggest that zerumbone exhibits anti-cancer activity by inducing lipid peroxidation and leading to biomolecular changes that result in apoptosis of NSCLC cells. Therefore, it was concluded that zerumbone may play a potential role in cancer treatment. However, further studies are needed to explain

the effect of zerumbone on biomolecular changes and also apoptotic pathways in cancer pathogenesis.

Author Contributions

All authors contributed to the study conception and design. Data collection, data analysis, and interpretation: Ç.Z.K., B.B., and D.Y. All authors wrote the main manuscript text and approved the manuscript.

Acknowledgments

The authors would like to thank Prof. Dr. Petek Korkusuz for her valuable support throughout the study. This work was supported by the Scientific Research Projects Fund of Yuksek Ihtisas University (project number 2021/01.005).

Conflicts of Interest

The authors declare no conflicts of interest.

Data Availability Statement

The data that support the findings of this study are available from the corresponding author upon reasonable request.

References

1. F. Bray, J. Ferlay, I. Soerjomataram, R. L. Siegel, L. A. Torre, and A. Jemal, "Global Cancer Statistics 2018: GLOBOCAN Estimates of Incidence and Mortality Worldwide for 36 Cancers in 185 Countries," *CA: A Cancer Journal for Clinicians* 68, no. 6 (2018): 394–424.

2. K. Zarogoulidis, P. Zarogoulidis, K. Darwiche, et al., "Treatment of Non-Small Cell Lung Cancer (NSCLC)," *Journal of Thoracic Disease* 5, no. Suppl. 4 (2013): S389.

3. Z. Hu, Q. Zeng, B. Zhang, H. Liu, and W. Wang, "Promotion of p53 Expression and Reactive Oxidative Stress Production Is Involved in Zerumbone-Induced Cisplatin Sensitization of Non-Small Cell Lung Cancer Cells," *Biochimie* 107, no. Part B (2014): 257–262.

4. S. H. Wu, L. W. Hang, J. S. Yang, et al., "Curcumin Induces Apoptosis in Human Non-Small Cell Lung Cancer NCI-H460 Cells Through ER Stress and Caspase Cascade- and Mitochondria-Dependent Pathways," *Anticancer Research* 30, no. 6 (2010): 2125–2133.

5. Y. C. Hseu, Y. C. Huang, M. Korivi, et al., "Zerumbone Attenuates TGF-β1-Mediated Epithelial-Mesenchymal Transition via Upregulated E-Cadherin Expression and Downregulated Smad2 Signalling Pathways in Non-Small Cell Lung Cancer (A549) Cells," *Journal of Functional Foods* 18 (2015): 58–72.

6. S. Girisa, B. Shabnam, J. Monisha, et al., "Potential of Zerumbone as an Anti-Cancer Agent," *Molecules* 24, no. 4 (2019): 734.

7. J. Li, L. Wang, Y. Sun, et al., "Zerumbone-Induced Reactive Oxygen Species-Mediated Oxidative Stress Re-Sensitizes Breast Cancer Cells to Paclitaxel," *Biotechnology and Applied Biochemistry* 70, no. 1 (2023): 28–37.

8. M. D. Ibáñez, N. M. Sánchez-Ballester, and M. A. Blázquez, "Healthy Zerumbone: From Natural Sources to Strategies to Improve Its Bioavailability and Oral Administration," *Plants* 12, no. 1 (2023): 5.

9. J. E. Jorvig and A. Chakraborty, "Zerumbone Inhibits Growth of Hormone Refractory Prostate Cancer Cells by Inhibiting JAK2/STAT3 Pathway and Increases Paclitaxel Sensitivity," *Anti-Cancer Drugs* 26, no. 2 (2015): 160–166.

10. C. G. Kang, H. J. Lee, S. H. Kim, and E. O. Lee, "Zerumbone Suppresses Osteopontin-Induced Cell Invasion Through Inhibiting the FAK/AKT/ROCK Pathway in Human Non-Small Cell Lung Cancer A549 Cells," *Journal of Natural Products* 79, no. 1 (2016): 156–160.

11. R. Prasannan, K. A. Kalesh, M. K. Shanmugam, et al., "Key Cell Signaling Pathways Modulated by Zerumbone: Role in the Prevention and Treatment of Cancer," *Biochemical Pharmacology* 84, no. 10 (2012): 1268–1276.

12. N. A. Wani, B. Zhang, K. y. Teng, et al., "Reprograming of Glucose Metabolism by Zerumbone Suppresses Hepatocarcinogenesis," *Molecular Cancer Research* 16, no. 2 (2018): 256–268.

13. S. I. Abdelwahab, A. B. Abdul, Z. N. M. Zain, and A. H. A. Hadi, "Zerumbone Inhibits Interleukin-6 and Induces Apoptosis and Cell Cycle Arrest in Ovarian and Cervical Cancer Cells," *International Immunopharmacology* 12, no. 4 (2012): 594–602.

14. S. Zhang, Q. Liu, Y. Liu, H. Qiao, and Y. Liu, "Zerumbone, a Southeast Asian Ginger Sesquiterpene, Induced Apoptosis of Pancreatic Carcinoma Cells Through p53 Signaling Pathway," *Evidence-Based Complementary and Alternative Medicine* 2012 (2012): 1–8.

15. N. Muhammad Nadzri, A. B. Abdul, M. A. Sukari, et al., "Inclusion Complex of Zerumbone With Hydroxypropyl-β-Cyclodextrin Induces Apoptosis in Liver Hepatocellular HepG2 Cells via Caspase 8/BID Cleavage Switch and Modulating Bcl2/Bax Ratio," *Evidence-Based Complementary and Alternative Medicine* 2013 (2013): 1–16.

16. M. Hosseinpour, A. B. Abdul, H. S. Rahman, et al., "Comparison of Apoptotic Inducing Effect of Zerumbone and Zerumbone-Loaded Nanostructured Lipid Carrier on Human Mammary Adenocarcinoma MDA-MB-231 Cell Line," *Journal of Nanomaterials* 2014 (2014): 742738.

17. H. S. Rahman, A. Rasedee, A. B. Abdul, et al., "Zerumbone-Loaded Nanostructured Lipid Carrier Induces G2/M Cell Cycle Arrest and Apoptosis via Mitochondrial Pathway in a Human Lymphoblastic Leukemia Cell Line," *International Journal of Nanomedicine* 9, no. 1 (2014): 527–538.

18. M. A. Haque, I. Jantan, L. Arshad, and S. N. A. Bukhari, "Exploring the Immunomodulatory and Anticancer Properties of Zerumbone," *Food & Function* 8, no. 10 (2017): 3410–3431.

19. J. Saranya, B. P. Dhanya, G. Greeshma, K. V. Radhakrishnan, and S. Priya, "Effects of a New Synthetic Zerumbone Pendant Derivative (ZPD) on Apoptosis Induction and Anti-Migratory Effects in Human Cervical Cancer Cells," *Chemico-Biological Interactions* 278 (2017): 32–39.

20. A. Rosa, D. Caprioglio, R. Isola, M. Nieddu, G. Appendino, and A. M. Falchi, "Dietary Zerumbone From Shampoo Ginger: New Insights Into Its Antioxidant and Anticancer Activity," *Food & Function* 10, no. 3 (2019): 1629–1642.

21. M. Redza-Dutordoir and D. A. Averill-Bates, "Activation of Apoptosis Signalling Pathways by Reactive Oxygen Species," *Biochimica et Biophysica Acta, Molecular Cell Research* 1863, no. 12 (2016): 2977–2992.

22. K. Zabłocka-Słowińska, S. Płaczkowska, K. Skórska, et al., "Oxidative Stress in Lung Cancer Patients Is Associated With Altered Serum Markers of Lipid Metabolism," *PLoS One* 14, no. 4 (2019): e0215246.

23. A. Ayala, M. F. Muñoz, and S. Argüelles, "Lipid Peroxidation: Production, Metabolism, and Signaling Mechanisms of Malondialdehyde and 4-Hydroxy-2-Nonenal," *Oxidative Medicine and Cellular Longevity* 2014 (2014): 1–31.

24. Y. Li, T. Zhao, J. Li, et al., "Oxidative Stress and 4-Hydroxy-2-Nonenal (4-HNE): Implications in the Pathogenesis and Treatment of Aging-Related Diseases," *Journal of Immunology Research* 2022 (2022): 2233906.

25. R. K. Sahu and S. Mordechai, "Fourier Transform Infrared Spectroscopy in Cancer Detection," *Future Oncology* 1, no. 5 (2005): 635–647.

26. D. Naumann, H. Fabian, and P. Lasch, "FTIR Spectroscopy of Cells, Tissues and Body Fluids," in *Biological and Biomedical Infrared Spectroscopy*, eds. A. Barth and P. I. Haris (Amsterdam, Netherlands: IOS Press, 2009), 312–354.

27. H. Liu, Q. Su, Q. Wu, et al., "FTIR Spectroscopic Study on Apoptosis of Lung Cancer Cell Line A549 Induced by Arsenic Trioxide," *Infrared Physics & Technology* 93 (2018): 340–345.

28. B. R. Shakya, H. R. Teppo, and L. Rieppo, "Discrimination of Melanoma Cell Lines With Fourier Transform Infrared (FTIR) Spectroscopy," *Spectrochimica Acta Part A: Molecular and Biomolecular Spectroscopy* 254 (2021): 119665.

29. B. B. Wu, Y. P. Gong, X. H. Wu, et al., "Fourier Transform Infrared Spectroscopy for the Distinction of MCF-7 Cells Treated With Different Concentrations of 5-Fluorouracil," *Journal of Translational Medicine* 13, no. 1 (2015): 108.

30. M. Kim, S. Miyamoto, Y. Yasui, T. Oyama, A. Murakami, and T. Tanaka, "Zerumbone, a Tropical Ginger Sesquiterpene, Inhibits Colon and Lung Carcinogenesis in Mice," *International Journal of Cancer* 124, no. 2 (2009): 264–271.

31. M. M. Bradford, "A Rapid and Sensitive Method for the Quantitation of Microgram Quantities of Protein Utilizing the Principle of Protein-Dye Binding," *Analytical Biochemistry* 72, no. 1–2 (1976): 248–254.

32. M. L. Chan, J. W. Liang, L. C. Hsu, W. L. Chang, S. S. Lee, and J. H. Guh, "Zerumbone, a Ginger Sesquiterpene, Induces Apoptosis and Autophagy in Human Hormone-Refractory Prostate Cancers Through Tubulin Binding and Crosstalk Between Endoplasmic Reticulum Stress and Mitochondrial Insult," *Naunyn-Schmiedeberg's Archives of Pharmacology* 388, no. 11 (2015): 1223–1236.

33. C. Nathaniel, Y. L. Elaine-Lee, B. C. Yee, et al., "Zerumbone-Loaded Nanostructured Lipid Carrier Induces Apoptosis in Human Colorectal Adenocarcinoma (Caco-2) Cell Line," *Nanoscience and Nanotechnology Letters* 8, no. 4 (2016): 294–302.

34. E. E. M. Eid, A. S. Alanazi, S. Koosha, et al., "Zerumbone Induces Apoptosis in Breast Cancer Cells by Targeting αvβ3 Integrin Upon Co-Administration With TP5-iRGD Peptide," *Molecules* 24, no. 14 (2019): 2554.

35. S. Behzad, K. Ebrahim, M. Mosaddegh, and A. Haeri, "Primula Auriculata Extracts Exert Cytotoxic and Apoptotic Effects Against HT-29 Human Colon Adenocarcinoma Cells," *Iran Journal of Pharmacy Research* 15, no. 1 (2016): 311.

36. M. Barathan, K. M. Vellasamy, Z. A. Ibrahim, V. Mariappan, S. M. Hoong, and J. Vadivelu, "Zerumbone Mediates Apoptosis and Induces Secretion of Proinflammatory Cytokines in Breast Carcinoma Cell Culture," *Iranian Journal of Basic Medical Sciences* 24, no. 11 (2021): 1538.

37. F. Gentile, A. Arcaro, S. Pizzimenti, et al., "DNA Damage by Lipid Peroxidation Products: Implications in Cancer, Inflammation and Autoimmunity," *AIMS Genetics* 04, no. 2 (2017): 103–137.

38. G. Bianchi, S. Ravera, C. Traverso, et al., "Curcumin Induces a Fatal Energetic Impairment in Tumor Cells In Vitro and In Vivo by Inhibiting ATP-Synthase Activity," *Carcinogenesis* 39, no. 9 (2018): 1141–1150.

39. J. G. Wang, D. L. Li, R. Fan, and M. J. Yan, "Zerumbone Combined With Gefitinib Alleviates Lung Cancer Cell Growth Through the AKT/STAT3/SLC7A11 Axis," *Neoplasma* 70, no. 1 (2023): 58–70.

40. Q. Yao, M. Lin, Y. Wang, et al., "Curcumin Induces the Apoptosis of A549 Cells via Oxidative Stress and MAPK Signaling Pathways," *International Journal of Molecular Medicine* 36, no. 4 (2015): 1118–1126.

41. F. Severcan and P. I. Haris, "Introduction to Vibrational Spectroscopy in Diagnosis and Screening," in *Vibrational Spectroscopy in Diagnosis and Screening*, eds. F. Severcan and P. I. Haris (Netherlands: IOS Press, 2012), 1–11.

42. N. Simsek Ozek, S. Tuna, A. E. Erson-Bensan, and F. Severcan, "Characterization of microRNA-125b Expression in MCF7 Breast Cancer Cells by ATR-FTIR Spectroscopy," *Analyst* 135 (2010): 3094.

43. U. Zelig, J. Kapelushnik, R. Moreh, S. Mordechai, and I. Nathan, "Diagnosis of Cell Death by Means of Infrared Spectroscopy," *Biophysical Journal* 97, no. 7 (2009): 2107–2114.

44. S. Gok, O. Kuzmenko, A. Babinskyi, and F. Severcan, "Vitamin E Derivative With Modified Side Chain Induced Apoptosis by Modulating the Cellular Lipids and Membrane Dynamics in MCF7 Cells," *Cell Biochemistry and Biophysics* 79, no. 2 (2021): 271–287.

45. G. Cakmak, M. Severcan, F. Zorlu, and F. Severcan, "Structural and Functional Damages of Whole Body Ionizing Radiation on Rat Brain Homogenate Membranes and Protective Effect of Amifostine," *International Journal of Radiation Biology* 92, no. 12 (2016): 837–848.

46. A. Derenne, O. Vandersleyen, and E. Goormaghtigh, "Lipid Quantification Method Using FTIR Spectroscopy Applied on Cancer Cell Extracts," *Biochimica et Biophysica Acta, Molecular and Cell Biology of Lipids* 1841, no. 8 (2014): 1200–1209.

47. D. Yonar and M. M. Sunnetcioglu, "Effect of Cis-(Z)-Flupentixol on DPPC Membranes in the Presence and Absence of Cholesterol," *Chemistry and Physics of Lipids* 198 (2016): 61–71.

48. D. Yonar, M. Severcan, R. Gurbanov, et al., "Rapid Diagnosis of Malignant Pleural Mesothelioma and Its Discrimination From Lung Cancer and Benign Exudative Effusions Using Blood Serum," *Biochimica et Biophysica Acta, Molecular Basis of Disease* 1868, no. 10 (2022): 166473.

49. R. K. Sahu, S. Argov, A. Salman, et al., "Characteristic Absorbance of Nucleic Acids in the Mid-IR Region as Possible Common Biomarkers for Diagnosis of Malignancy," *Technology in Cancer Research & Treatment* 3, no. 6 (2004): 629–638.

50. R. K. Sahu, A. Salman, and S. Mordechai, "Tracing Overlapping Biological Signals in Mid-Infrared Using Colonic Tissues as a Model System," *World Journal of Gastroenterology* 23, no. 2 (2017): 286–296.

51. P. L. Fale, A. Altharawi, and K. L. A. Chan, "In Situ Fourier Transform Infrared Analysis of Live Cells' Response to Doxorubicin," *Biochimica et Biophysica Acta, Molecular Cell Research* 1853, no. 10 (2015): 2640–2648.

52. F. Gasparri and M. Muzio, "Monitoring of Apoptosis of HL60 Cells by Fourier-Transform Infrared Spectroscopy," *Biochemical Journal* 369, no. 2 (2003): 239–248.

53. C. M. C. Andrés, J. M. P. d. l. Lastra, C. A. Juan, F. J. Plou, and E. Pérez-Lebeña, "Chemical Insights Into Oxidative and Nitrative Modifications of DNA," *International Journal of Molecular Sciences* 24, no. 20 (2023): 15240.

54. W. M. Przybyszewski, J. Kasperczyk, K. Stokłosa, and A. Bkhiyan, "DNA Damage Induced by Products of Lipid Peroxidation," *Postępy Higieny i Medycyny Doświadczalnej (Online)* 59 (2005): 75–81.

55. F. Guéraud, M. Atalay, N. Bresgen, et al., "Chemistry and Biochemistry of Lipid Peroxidation Products," *Free Radical Research* 44, no. 10 (2010): 1098–1124.

56. A. Winczura, D. Zdzalik, and B. Tudek, "Damage of DNA and Proteins by Major Lipid Peroxidation Products in Genome Stability," *Free Radical Research* 46, no. 4 (2012): 442–459.

57. C. E. Zois, E. Favaro, and A. L. Harris, "Glycogen Metabolism in Cancer," *Biochemical Pharmacology* 92, no. 1 (2014): 3–11.